Histone Variants H3.3 and H2A.Z/H3.3 Facilitate Excision of Uracil from Nucleosome Core Particles

Chuxuan Li, Katelyn L. Rioux, and Sarah Delaney*

Department of Chemistry, Brown University, Providence, RI, USA

*Correspondence to: Department of Chemistry, Brown University, Providence, RI, USA. Email address: Sarah_Delaney@brown.edu (S. Delaney)

Keywords: Nucleosome core particle; Base excision repair; Histone H2A.Z; Histone H3.3; Uracil DNA glycosylase; Single-strand selective monofunctional uracil DNA glycosylase

Graphical abstract

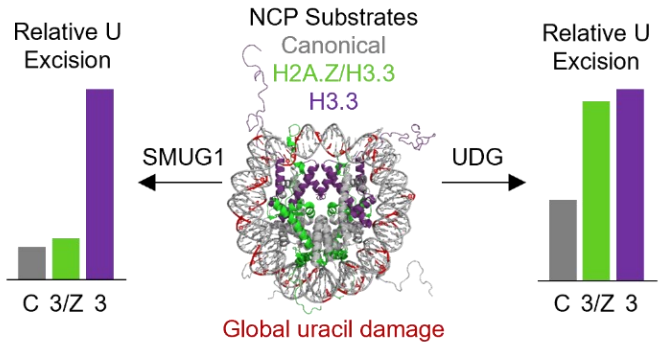

Highlights

- Histone variants modulate BER activity in nucleosome core particles
- Enhanced excision of uracil by UDG and SMUG1 is observed with the H3.3 variant
- Enhanced excision of uracil by UDG is observed with the H2A.Z/H3.3 double variant
- Octasome and hexasome species of H3.3 NCPs facilitate excision by UDG and SMUG1
- Most enhancement at sterically-occluded sites and terminal regions of the hexasome

ABSTRACT

At the most fundamental level of chromatin organization, DNA is packaged as nucleosome core particles (NCPs) where DNA is wound around a core of histone proteins. This ubiquitous sequestration of DNA within NCPs presents a significant barrier to many biological processes, including DNA repair. We previously demonstrated that histone variants from the H2A family facilitate excision of uracil (U) lesions by DNA base excision repair (BER) glycosylases. Here, we consider how the histone variant H3.3 and double-variant H2A.Z/H3.3 modulate the BER enzymes uracil DNA glycosylase (UDG) and single-strand selective monofunctional uracil DNA glycosylase (SMUG1). Using an NCP model system with U:G base pairs at a wide variety of geometric positions we generate the global repair profile for both glycosylases. Enhanced excision of U by UDG and SMUG1 is observed with the H3.3 variant. We demonstrate that these H3.3-containing NCPs form two species: (1) octasomes, which contain the full complement of eight histone proteins and (2) hexasomes which are sub-nucleosomal particles that contain six histones. Both the octasome and hexasome species facilitate excision activity of UDG and SMUG1, with the largest impacts observed at sterically-occluded lesion sites and in terminal regions of DNA of the hexasome that do not closely interact with histones. For the double-variant H2A.Z/H3.3 NCPs, which exist as octasomes, the global repair profile reveals that UDG but not SMUG1 has increased

U excision activity. The enhanced glycosylase activity reveals potential functions for these histone variants to facilitate BER in packaged DNA and contributes to our understanding of DNA repair in chromatin and its significance regarding mutagenesis and genomic integrity.

Abbreviations

BER, base excision repair; DTT, dithiothreitol; FD, free duplex DNA; FOXA1, forkhead box A1; H2A.Z/H3.3, H2A.Z/H3.3 double variant; H3.3, H3.3 variant; HRF, hydroxyl radical footprinting; MNase, micrococcal nuclease; NCP, nucleosome core particle; PAGE, polyacrylamide gel electrophoresis; PCI, phenol chloroform isoamyl alcohol; PCNA, proliferating cell nuclear antigen; PTMs, post-translational modifications; RPA2, replication protein A2; SAFA, semi-automated footprinting analysis; SE, standard error; SMUG1, single-strand selective monofunctional uracil DNA glycosylase; U, uracil; UDG, uracil DNA glycosylase

1. Introduction

Eukaryotic genomic DNA is packaged into nucleosome core particles (NCPs) to compact its structure. A single NCP is composed of a core of histone proteins wrapped by ~145 bp of DNA in ~1.7 superhelical turns (Figure 1A) [1]. The histone core is made up of two copies each of four proteins (H2A, H2B, H3, and H4). The histone proteins have maintained a high degree of conservation during evolution, indicative of their central role in the packaging of DNA. Furthermore, the histone genes are present in multiple copies in most organisms allowing for a degree of nonallelic variation. In fact, all eukaryotic organisms contain specialized histone variants with distinct amino acid sequences and expression patterns [2].

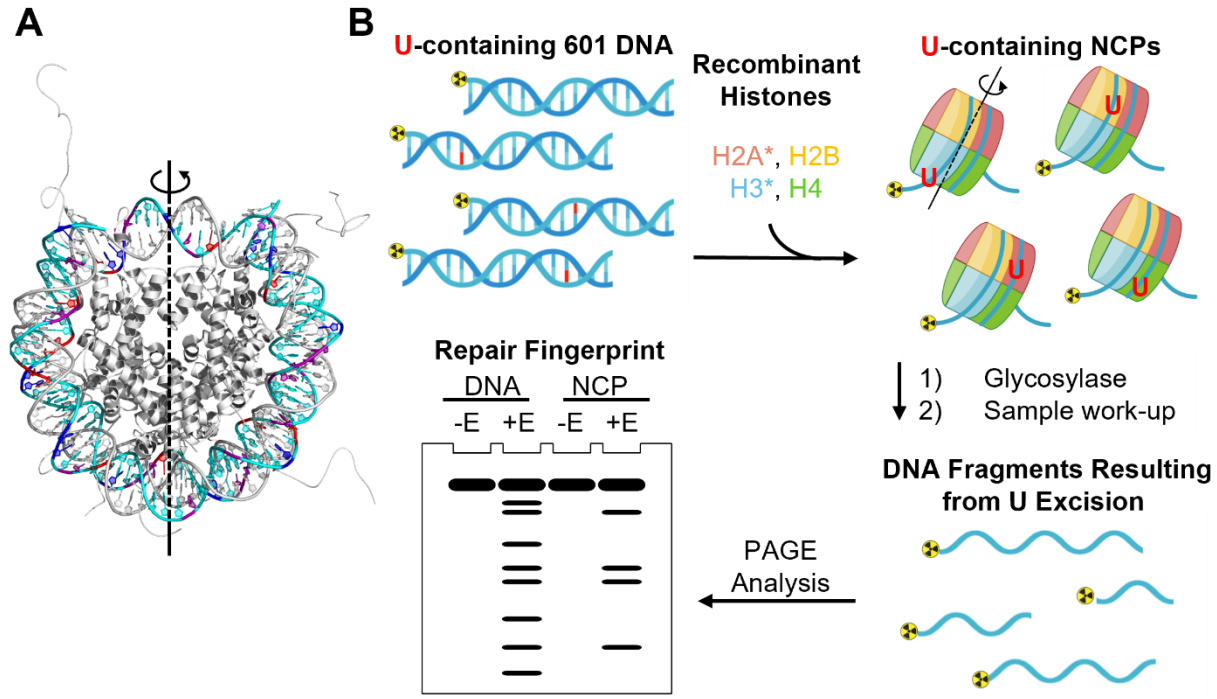

Figure 1. NCP model system is used to generate the repair fingerprint of a glycosylase enzyme. (A) U containing NCP model constructed by merging the crystal structure of an NCP containing Widom 601 DNA (PDB: 3lz0) with a canonical histone octamer containing histone tails (PDB: 1kx5). U sites are highlighted according to their solution accessibility determined by HRF (high: blue; intermediate: purple; low: red). Non-U sites of the 601 "I" strand are cyan. Dyad axis is indicated by a dashed line. (B) U lesions are globally incorporated into Widom 601 duplex DNA and reconstituted with recombinant canonical and variant histone proteins via salt dialysis to form

NCPs. U containing NCPs are treated with glycosylase and polyacrylamide gel electrophoresis (PAGE) analysis reveals sites that are repaired by BER in the repair fingerprint.

Whereas relatively few variants of H2B and H4 are known, most eukaryotes have several variants of H2A and H3 [2]. For example, the histone variants H2A.Z and H3.3 are known to be enriched at NCPs in actively transcribed genes [3-5]. The H2A.Z variant shares only ~60% homology with canonical H2A [6]. In fact, H2A.Z is one of the most divergent histone variants, but H2A.Z itself is well conserved across species. A crystal structure of an NCP containing H2A.Z revealed very little difference relative to a canonical NCP, although there are some changes in the interface between H2A.Z and the H3/H4 histones [7]. Nevertheless, NCPs containing H2A.Z are more sensitive to salt-mediated disruption, which is reflective of decreased stability and looser DNA packaging [8,9].

Several forms of H3 are expressed in higher eukaryotes: H3.1 (canonical), H3.2, H3.3 and CENP-A, which is a centromere-specific variant. Intriguingly, H3.3 differs from H3.1 and H3.2 by only five and four amino acids, respectively [10]. Three of those amino acids are clustered in the center of the polypeptide chain, and the critical role of these amino acids is highlighted by the fact that mutation of these residues alters the way H3.3 is deposited throughout the genome [10]. H3.1 and H3.2 are expressed during S phase and have been termed “DNA synthesis-coupled” because they are incorporated into newly replicated chromatin. In contrast, H3.3 has been termed a “replacement histone” as it is expressed throughout the cell cycle and is deposited into chromatin by distinct chaperones independent of DNA synthesis [11]. H3.3 is known to be deposited by histone chaperones involved with homologous recombination (HR) [12] and nucleotide excision repair (NER) [13]. Similar to H2A.Z, histone H3.3 also renders NCPs more sensitive to salt-mediated disruption [8,9].

Notably, it has been shown that double-variant NCPs containing both H3.3 and H2A.Z are enriched at transcription start sites in human cells and that these NCPs facilitate access of transcription factors to the packaged DNA [14]. In fact, these NCPs are sufficiently loosely packaged that they were lost using the early preparative techniques that isolated NCPs at higher salt conditions [14]. It was only when experiments were performed at lower salt concentrations that they were identified in cells. However, in other work, when isolated from vertebrates, immunoprecipitation studies have demonstrated that these dual-variant NCPs are at least as stable as canonical NCPs [8].

It has been proposed that DNA repair in chromatin occurs via an access-repair-restore model [15]. The looser packaging of DNA suggests that NCPs containing H3.3 and/or H2A.Z variants could be a way for cells to regulate and facilitate access to DNA for repair. In previous work we demonstrated that H2A.Z facilitates DNA repair via the base excision repair (BER) pathway [16]. Here, using uracil (U) as a representative lesion repaired by BER, we explored the ability of H3.3 and the double variant H2A.Z/H3.3 to modulate initiation of this repair pathway by two uracil DNA glycosylases: uracil DNA glycosylase (UDG) and single-strand selective monofunctional uracil DNA glycosylase (SMUG1). UDG and SMUG1 are the two major glycosylases responsible for excising U from U:G base pairs and it was recently reported that accumulation of U in CpG sites arises primarily from cytosine deamination in mice lacking UDG and SMUG1 [17]. We find that the H3.3 variant facilitates activity of both glycosylases, and that the presence of both H2A.Z/H3.3 facilitates UDG, but not SMUG1.

2. Materials and methods

2.1 Oligonucleotide synthesis and purification

All DNA was synthesized on a MerMade 4 (BioAutomation) DNA synthesizer using phosphoramidite chemistry. Phosphoramidites were purchased from Glen Research. The 145 bp Widom 601 sequence [18] was used for all duplex control and NCP samples (Scheme S1). The U containing lesion strand (LS_U) was synthesized as previously reported using C phosphoramidite spiked with a small amount of U [19]. The molar ratio used to create the C/U mixture was determined by the Poisson distribution (λ=0.355) to ensure that 95% of DNA contained no more than one U per strand. The DNA was purified by 8% denaturing polyacrylamide gel electrophoresis (PAGE). Nucleobases are numbered from 1 to 145 starting from the 5′-end of the U-containing strand.

The 145-mer complement strand (CS) was prepared via ligation of shorter component strands using T4 ligase (New England Biolabs) in the presence of scaffold DNA strands (Scheme S2). Component and scaffold strands were synthesized with final trityl group intact for reverse-phase HPLC purification (Dynamax Microscorb C18 column, 250 x 10 mm; A = acetonitrile [MeCN], B = 30 mM NH_4OAc; 5:95 to 35:65 A:B over 30 min at 3.5 mL/min). The trityl group was removed by incubation in 20% v/v aqueous glacial acetic acid for 1 h at ambient temperature, followed by a second round of HPLC purification at 90 °C (Agilent PLRP-S column, 250 x 4.6 mm; A = 100 mM triethylammonium acetate [TEAA] in 5% aqueous MeCN, B = 100 mM TEAA in MeCN; 0:100 to 15:85 A:B over 35 min then 15:85 to 35:65 A:B over 5 min at 1 mL/min). Electrospray ionization mass spectrometry was used to confirm the identity of component and scaffold strands. The ligated CS was purified by 8% denaturing PAGE.

Two single-stranded internal standards, used for normalization and loading controls, were designed as a 30-mer and a 98-mer (Scheme S1) such that they would not co-migrate with any U

cleavage product. These strands were synthesized with the final trityl group removed and purified by 12% and 8% denaturing PAGE, respectively.

2.2 Histone preparation, NCP reconstitution, heat-shifting assay

Canonical *X. laevis* histones (H2A, H2B, H3.1, H4) were recombinantly expressed and purified according to published protocols [20]. Throughout this work "canonical H3" refers to H3.1. Human H2A.Z and H3.3 were purchased from the Histone Source (Colorado State University). Canonical H2A/H3, H2A.Z/H3.3, and H2A/H3.3 containing octamers were individually assembled and purified [20] and the corresponding NCPs were then reconstituted via salt-gradient dialysis as previously described [20,21]. This assembly process yields homotypic NCP populations in which both copies of the canonical histone are replaced with the respective variant. LS_U was 5′-^{32}P-radiolabeled and annealed to CS in annealing buffer (10 mM Tris [pH 8], 50 mM NaCl, 1 mM EDTA). In an equimolar ratio, 1 µM duplex DNA was mixed with the relative octamer at 4 °C in 2 M NaCl, 10 mM Tris-HCl (pH 7.5), 1 mM EDTA, 1 mM dithiothreitol (DTT) and 500 µg/mL BSA. The NaCl concentration was reduced stepwise at 1 h intervals (1.2, 1.0, 0.6 and 0 M) via dialysis, and the final dialysis into 0 M was carried out for 3 h. NCPs were then filtered by centrifugation using a Spin-X Centrifuge Tube filter (0.22 µm, Corning Incorporated) to remove precipitates, and the purity of samples was evaluated by 7% native PAGE (19:1 acrylamide:bisacrylamide, 4° C, 3 h, 150 V, 0.25X TBE). Only NCPs with high purity (<5% duplex DNA) were used in subsequent experiments. In the heat shifting assay, NCPs were incubated at 37 °C or 55 °C for 1 h and subjected to 7% native PAGE immediately at 4 °C.

Octasome and hexasome species of H3.3 NCPs were purified by Mini Prep Cell (Bio-Rad Laboratories) on a 7%, 7 cm gel (19:1 acrylamide:bisacrylamide; 4° C, 6 h, 360 V). Fractions of

360 µL were collected with an elution rate of 120 µL/min, then visualized on a 7% native PAGE (19:1 acrylamide:bisacrylamide; 4 °C, 3 h, 150 V, 0.25X TBE). Pure fractions for each species were combined and concentrated with an Amicon Ultra 30K MWCO concentrator. Purified samples were visualized by 7% native PAGE (19:1 acrylamide:bisacrylamide; 4° C, 3 h, 150 V, 0.25X TBE).

2.3 Global assessment of UDG and SMUG1 activity

Similar to other studies that examined U excision from NCPs [22,23], we used *E. coli* UDG which is 73% similar to human UNG with a conserved active site [24]. Comparison of the crystal structures of *E. coli* UDG and human UNG shows the overall shapes are highly similar [25]. *E. coli* UDG and human SMUG1 were purchased from New England Biolabs. The total concentration of each glycosylase was determined by Bradford assay using γ-globulin standards (Bio-Rad Laboratories). To assess glycosylase activity, 0.5 pmol substrate (global U containing duplex DNA or NCPs) were mixed with 10 pmol UDG or SMUG1 in a total volume of 20 µL of the glycosylase reaction buffer (20 mM Tris-HCl [pH 7.6], 50 mM NaCl, 150 mM KCl, 1 mM EDTA, 1 mM DTT, 200 µg/mL BSA). Samples were incubated for 1 h at 37 °C. A negative control sample (-E) was also incubated for 1 h at 37 °C, but with no enzyme present to reveal any pre-existing damage or incidental damage of the substrate before and during the reaction. Reactions were quenched with equal volume (20 µL) of 1 M NaOH and heated for 2 min at 90 °C. The NaOH quench solution was spiked with 5′-^{32}P-radiolabeled internal standards prior to addition to samples. DNA fragments were then extracted from proteins using 25:24:1 phenol:chloroform:isoamyl alcohol (PCI). No significant detection of radioactivity in the organic phase indicates that stable DNA-histone crosslinks are not forming under these experimental conditions. The DNA was precipitated from the aqueous phase by addition of 40 µL co-precipitation agent (0.3 M NaOAc, 1 mM EDTA, 0.5

mg/mL tRNA) and 600 µL ethanol and incubation overnight at -20 °C. The precipitated sample was resuspended in 50% v/v formamide and split in half. One half of the sample was loaded onto a 10% denaturing PAGE gel (0.4 mm, 2 h, 85 W, 1X TBE) to resolve bands from nucleobase 9 to the dyad axis and the other half loaded onto an 8% gel (0.4 mm, 3 h, 85 W, 1X TBE) to resolve bands from the dyad axis to nucleobase 129. Gels were imaged by phosphorimagery (Bio-Rad PharosFX).

SAFA software [26] was used to quantitate band intensity. To account for any differences in sample loading, band intensities were normalized using the intensities of the internal standards (30-mer for the 10% gel and 98-mer for the 8% gel). Negative control (-E) samples were subtracted from the glycosylase-treated samples. At each U site, the ratio of corrected band intensity observed for NCPs to duplex DNA was determined. The standard error (SE) of NCP/FD was calculated using the equation $SE = \sigma/\sqrt{n}$ where σ is the standard deviation and n is the sample size (n =3). A two-tailed Welch's *t* test (α = 0.05) was performed to obtain the *p* value at each U site for each variant NCP in comparison to canonical NCP/FD. All statistical analyses were conducted using R. We considered $p < 0.05$ to be significant.

2.4 Hydroxyl radical footprinting (HRF)

Based on previously published methods [27,28], HRF reactions were performed on duplex DNA and NCPs to determine solution accessibility at each nucleobase position. Briefly, 7.5 µL of each 10 mM Fe(II)-EDTA, 10 mM sodium ascorbate, and 0.12% w/v aqueous hydrogen peroxide were combined and immediately added to 5 pmol of duplex DNA or NCPs in 52.5 µL of reaction buffer (10 mM Tris-HCl, [pH 7.5], 1 mM EDTA). The reaction was incubated in the dark at ambient temperature for 2 min (duplex DNA) or 10 min (NCPs) and was quenched with the addition of 16 µL 50 mM EDTA in 25% v/v glycerol. Duplex DNA underwent ethanol

precipitation by addition of 50 µL of 7.5 M NH_4OAc and 600 µL of ethanol. NCP samples were immediately run on a 7% native PAGE to separate NCPs from duplex DNA that disassociated during the reaction. The NCP band was excised from the gel and eluted into buffer (0.3 M NaOAc, 1 mM Tris-HCl [pH 8.0], 1 mM EDTA) overnight at 37 °C with gentle shaking. The eluent was concentrated and extracted twice against PCI. DNA fragments in the resulting aqueous phase were purified via ethanol precipitation. Samples were resuspended in 50% v/v formamide, split in half, and half loaded onto a 10% denaturing PAGE to resolve bands 8-82 and half loaded onto an 8% gel to resolve bands 83-130. Gels were imaged by phosphorimagery, and bands were quantified using SAFA software. To determine the solution accessibility of each nucleobase, we first identified the highest HRF reactivity within a helical turn of nucleosomal DNA. The ratio of band intensity at each nucleobase position within this helical turn was then obtained by dividing the HRF value at a given position by the highest HRF reactivity. Positions with a ratio greater than 0.8, ranging from 0.8-0.2, and below 0.2 were assigned as sites that have high, intermediate, and low solution accessibility, respectively.

2.5 Micrococcal nuclease (MNase) digestion

1 pmol of NCPs was treated with 1, 4, or 20 units of MNase (New England Biolabs) in 20 µL of MNase reaction buffer (50 mM Tris-HCl [pH 7.5], 5 mM $CaCl_2$, 100 µg/mL BSA) for 5 min at ambient temperature. MNase was inactivated by incubation at 37 °C for 30 min with the addition of 20 µL of stop solution (50 mM Tris-HCl [pH 7.5], 200 mM EDTA, 0.25% w/v SDS and 0.5 mg/mL proteinase K). DNA fragments were then extracted against PCI and desalted by ethanol precipitation. 8% denaturing PAGE was used to visualize and analyze cleavage of nucleosomal DNA from MNase digestion.

3. Results

3.1 Reconstitution of NCPs containing global U:G mispairs

We utilized the NCP as a model system to study the repair profile of UDG and SMUG1 in packaged DNA (Figure 1B). NCP substrates were prepared based on the Widom 601 duplex sequence [29]. Structural information and previous biochemical characterizations of 601 NCPs are available and define the features of NCPs that may affect DNA accessibility for repair [18,30]. The 601 sequence is a strong positioning sequence that binds to the histone octamer in a unique, reproducible manner, creating a homogenous population of NCPs. The DNA in an NCP can be described based on its rotational and translational position. The rotational position refers to the locations of the major and minor grooves with respect to the histones, while the translational position refers to the distance from the dyad axis (Figure 1A), which is a two-fold axis of pseudosymmetry in the NCP.

Using synthetic methods described previously, U lesions were globally incorporated into the "I strand" of the 601 duplex [16,19,31]. A population of DNA with an unbiased distribution of U:G mispairs was generated with 95% of the duplexes containing at most one U. Using this population of duplex DNA and recombinant histones, three NCP substrates were reconstituted via salt gradient dialysis [20]: (1) canonical NCPs, (2) H3.3-containing NCPs (H3.3 NCP), and (3) double-variant NCPs containing both H3.3 and H2A.Z (H2A.Z/H3.3 NCP). Important for the work described here, while when probed by salt-mediated disruption NCPs containing both variants are destabilized relative to those containing only a single variant, they can be assembled *in vitro* [32].

The purity of the NCPs was evaluated using native PAGE. While canonical and H2A.Z/H3.3 NCPs migrate as a single species, H3.3 NCPs migrate as two species (Figure 2). The slower migrating species composes 60% of the sample, while the faster migrating species

composes 40%. Similar observations for H3.3 NCPs constructed using longer DNA sequences was reported previously and was attributed to two different translational positions of the DNA [32]. Therefore, we performed a heat-shifting assay, in which NCPs with different translational positions can potentially be converted to the thermodynamically favored position. Incubation of H3.3 NCPs at 37 ℃ or 55 ℃ does not induce re-distribution of the two bands (Figure S1), indicating that H3.3 NCPs exists as two distinct populations that are thermodynamically stable and are not interchangeable under the experimental conditions.

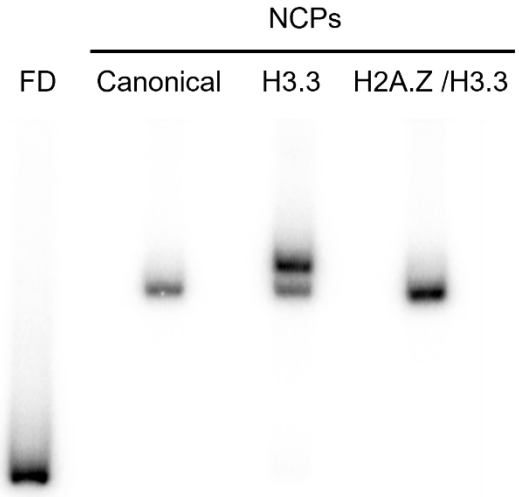

Figure 2. Representative native PAGE analysis of U containing canonical, H3.3-containing (H3.3), and H2A.Z/H3.3 double variant containing (H2A.Z/H3.3) NCPs relative to the U-containing duplex control (FD).

3.2 Verification of lesion solution accessibility in NCPs by hydroxyl radical footprinting

The NCPs prepared with global U-containing DNA present lesions in a variety of translational and rotational positions. To define the solution accessibility at each lesion site, we performed hydroxyl radical footprinting (HRF) experiments in which hydroxyl radicals non-discriminatively cleave the DNA backbone at solution-accessible sites via abstraction of hydrogen atoms from the deoxyribose ring [27]. In NCPs, portions of the deoxyribose-phosphate backbone

that connect to nucleobases facing outward from the histones are highly solution-accessible and susceptible to cleavage by hydroxyl radicals. In contrast, portions of the backbone that connect to nucleobases facing inward toward the histones are protected from hydroxyl radicals. The HRF profile of canonical NCPs, therefore, displays an oscillatory pattern of cleavage as the DNA wraps toward and away from the histone protein core (Figure S2).

The solution accessibility at each U lesion was quantified and normalized to the highest HRF reactivity within each ~10 base pair helical turn. Sites with values of greater than 0.8, 0.8-0.2, and less than 0.2 were defined as high (HIGH), intermediate (MID), and low (LOW) solution accessibility, respectively (Table S1). With the strategy of global lesion incorporation, we obtained a population of NCPs with 46 U lesions positioned at diverse translational positions and of varied levels of solution accessibility, allowing for the identification of the repair fingerprint of glycosylases in the context of packaged DNA.

3.3 Enhanced excision activity of UDG on H3.3 and H2A.Z/H3.3 NCPs

Given the fact that U can be efficiently excised by UDG from duplex DNA that is not incorporated into NCPs, we utilized duplex DNA as a positive control for activity of the glycosylase (Figure 3A and 3B; Lanes FD+E). The appearance of bands reflects excision of U. As expected, excision is observed at all sites of U incorporation throughout the sequence for duplex DNA. At each lesion site, the ratio of U excision from NCPs compared to duplex DNA was determined and plotted versus nucleobase position to generate the repair fingerprint (Figure 4A, bar graph). A ratio of 1 indicates comparable glycosylase activity in NCPs relative to duplex DNA, while a ratio of less than 1 reflects hindered enzymatic performance in NCPs. The HRF profile of

nucleobases in the NCP is also displayed to show the solution accessibility of each U site (Figure 4A, background gray).

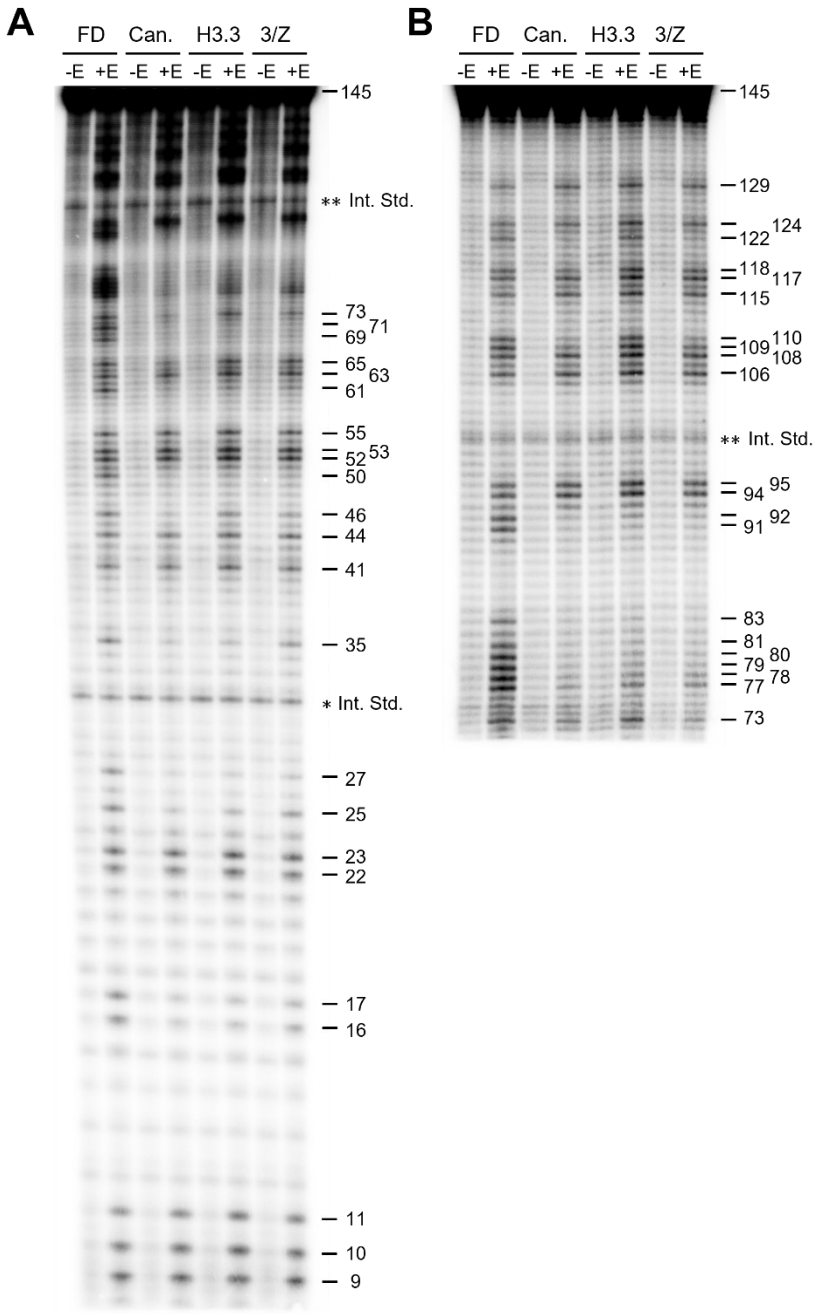

Figure 3. Representative PAGE gel showing U excision from Widom 601 "I" strand duplex (FD), canonical NCPs (Can.), H3.3 containing NCPs (H3.3), and H2A.Z/H3.3 double variant containing NCPs (3/Z) by UDG (+E). Negative control (-E) lanes, treated with NaOH only, indicate any pre-existing and incidental damage occurred before the experiments or during sample workup. Internal

standards, indicated with asterisks, are used for normalization. (A) 5′-end of 601 “I” strand. (B) 3′-end of 601 “I” strand.

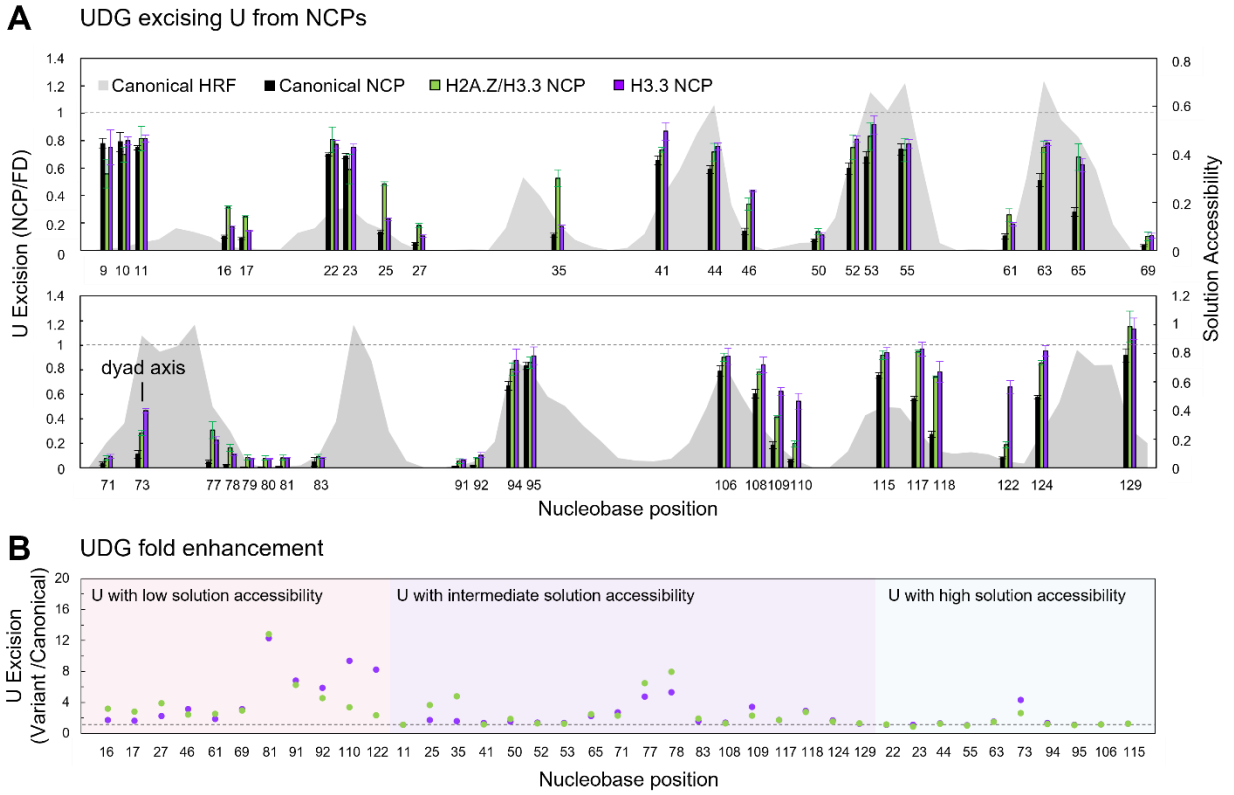

Figure 4. Excision of U from NCPs containing global C to U substitution after incubation with UDG. (A) At each U site, the ratio of product yield in NCPs to that in duplex DNA (FD) is plotted versus nucleobase position (canonical NCPs, black; H2A.Z/H3.3 NCPs, green; H3.3 NCPs, purple). A ratio of 1, indicated by a dotted line, represents a case in which excision of U from NCPs is as efficient as in duplex DNA. The dyad axis is indicated at position 73. Solution accessibility of each nucleobase position is shown by the HRF profile (gray area). Error bars represent standard error (n=3). (B) UDG excision of U from H2A.Z/H3.3 NCP (green) and H3.3 NCP (purple) relative to canonical NCP. A ratio of >1 means that U removal is facilitated in the variant NCP substrate. Positions at which the canonical excision ratio is 0, are omitted because the resulting fold enhancement value is undefined.

Consistent with our previous work, we found that the extent of U excision by UDG from canonical NCPs substantially correlates to the solution accessibility of U (Figure 4A, black bars). Most HIGH positions exhibit significant UDG activity with repair ratios ranging between 0.6 and 1 (sites 22, 23, 44, 55, 94, 95, 106, and 115). Conversely, minimal U excision was observed at most LOW positions with ratios of <0.15 (sites 16, 17, 27, 46, 61, 69, 81, 91, 92, 110, and 122).

Notably, exceptions to the correlation between UDG activity and solution accessibility were observed in the region near the dyad axis (which is centered at position 73), where U excision is largely suppressed regardless of solution accessibility.

Of interest, in H3.3 NCPs, while most HIGH positions still exhibit efficient U excision, multiple LOW and MID positions display enhanced UDG activity compared to canonical NCPs (sites 46, 77, 78, 81, 83, 109, 110, 117, 122, and 124) (Figure 4A, purple bars). Additionally, whereas the region near the dyad axis remains inhibitory to UDG activity, it is notable that there is a small but overall enhancement of U excision in this region, especially at site 73 with a ratio approaching 0.5. Moreover, starting from site 108 to the last examined lesion site of 129, U excision is efficient at all lesion positions regardless of solution accessibility; a 3 to 9-fold increase in UDG activity was observed at sites 109, 110, 118, and 122 relative to canonical NCPs.

In H2A.Z/H3.3 NCP, the correlation between UDG activity and solution accessibility is generally retained (Figure 4A, green bars). Similar to the repair fingerprint observed for H3.3 NCPs, several MID and LOW positions exhibit higher degree of U excision by UDG in H2A.Z /H3.3 NCPs relative to canonical NCPs, with notable differences at sites 16, 17, 25, 27, 35, 78, 92, 110, 117, 118, and 122. Relative to canonical NCPs, the inhibition of UDG activity in the dyad region is slightly alleviated.

The relative fold enhancement of excision of U by UDG from H2A.Z/H3.3 (green dots) and H3.3 (purple dots) NCPs relative to canonical NCPs is summarized in Figure 4B. A value of 1 means that the histone variant(s) does not alter glycosylase activity at that position whereas a value greater than 1 reflects enhanced U excision in the presence of the variant(s). A complete list of fold enhancement values of each position from each NCP substrate can be found in Table S2 for UDG.

3.4 Enhanced excision activity of SMUG1 on H3.3 NCP

U excision by SMUG1 is largely suppressed in both canonical and H2A.Z/H3.3 NCPs, as seen from the minimal excision observed at almost all lesion sites (Figure 5A, black and green bars; Figure S3). Efficient U removal was observed only at site 11, which is close to the DNA entry/exit region, and at site 95, which is highly solution accessible as determined by HRF. In H3.3 NCPs (Figure 5A, purple bars), enhanced SMUG1 activity is observed at sites 10, 16, 17, 22, 23, 25, 27, 41, 44, 52, 63, 78, 80, 81, 91, 92, 94, and 95. The absolute values of these changes are small but significant compared to canonical NCPs. In H3.3 NCPs, relative to canonical NCPs, the inhibition of SMUG1 activity at the dyad region is slightly alleviated. Similar to the UDG repair profile, high levels of U excision with ratios of greater than 0.6 was observed at all lesion positions in the region from site 106 to 129 in H3.3 NCPs (Table S3). The relative fold enhancement of excision of U by SMUG1 from H2A.Z/H3.3 (green dots) and H3.3 (purple dots) NCPs relative to canonical NCPs is summarized in Figure 5B. A complete list of fold enhancement values of each position from each NCP substrate can be found in Table S3 for SMUG1.

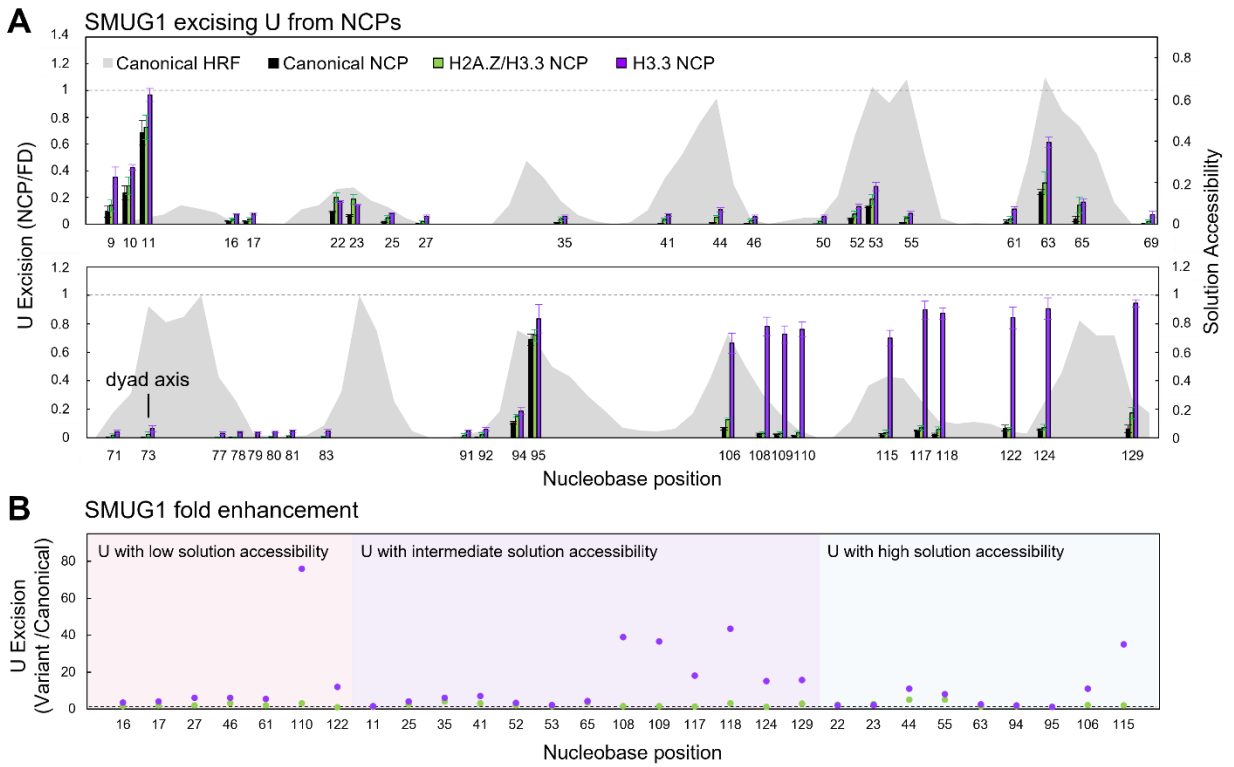

Figure 5. Excision of U from NCPs containing global C to U substitution after incubation with SMUG1. (A) At each U site, the ratio of product yield in NCPs to that in duplex DNA (FD) is plotted versus nucleobase position (canonical NCPs, black; H2A.Z/H3.3 NCPs, green; H3.3 NCPs, purple). A ratio of 1, indicated by a dotted line, represents a case in which excision of U from NCPs is as efficient as in duplex DNA. The dyad axis is indicated at position 73. Solution accessibility of each nucleobase position is shown by the HRF profile (gray area). Error bars represent standard error (n=3). (B) SMUG1 excision of U from H2A.Z/H3.3 NCP (green) and H3.3 NCP (purple) relative to canonical NCP. A ratio of >1 means that U removal is facilitated in the variant NCP substrate. Positions at which the canonical excision ratio is 0, are omitted because the resulting fold enhancement value is undefined.

3.5 H3.3 NCPs are a mixture of octasomes and hexasomes

To identify the two species of H3.3 NCPs observed by native PAGE, the species were purified using a Mini Prep Cell (Figure S4) and separately characterized by HRF and micrococcal nuclease (MNase) digestion. For the faster-migrating species, which co-migrates with canonical NCPs, an oscillatory pattern of HRF cleavage is observed for the entire DNA sequence (Figure 6, pink; Figure S5). In contrast, from site 115 to the end of the DNA sequence, the slower-migrating species exhibits high susceptibility towards hydroxyl radicals indicating much weaker interaction

or loss of contact between the DNA and the protein core (Figure 6, blue; Figure S5). This data is consistent with the slower-migrating species being less compact and one in which only ~115 bp of DNA is tightly associated with the histone core. Notably, this region is also where UDG and SMUG1 activity are facilitated.

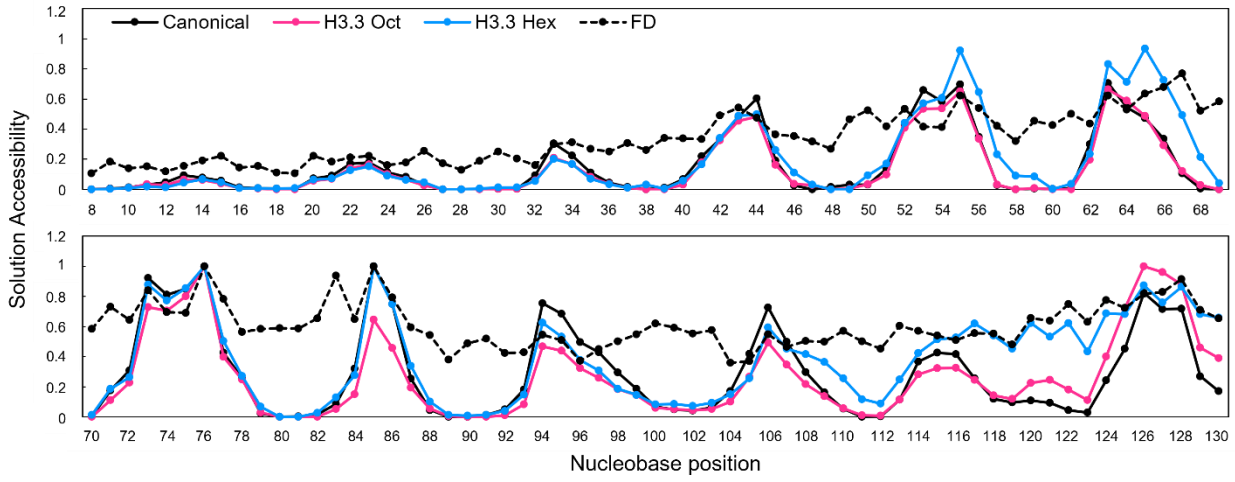

Figure 6. Hydroxyl radical footprinting of DNA in canonical and H3.3 variant NCPs as well as free duplex DNA. The band intensity at each nucleobase position on the denaturing PAGE gel (Figure S5) was quantified and normalized. The varying solution accessibility across the sequence of each sample (canonical NCP, solid black; H3.3 octasome, pink; H3.3 hexasome, blue; free duplex (FD), dashed black) is shown.

MNase preferentially digests DNA that is not closely associated with the histone core. For canonical NCPs, the most prominent fragment is a 128-mer, indicating that 17 bp of DNA were digested at the 3′-end of the I strand, due to transient unwrapping in the entry/exit region (Figure 7). In comparison, cleavage at sites 102, 103, and 110 is unique to H3.3 NCPs (Figure 7, dashed boxes). Notably, the 110-mer fragment is observed even at low Mnase concentration, indicating a weak interaction between the histone core and the 35 bp of DNA at the 3′-end of the I strand.

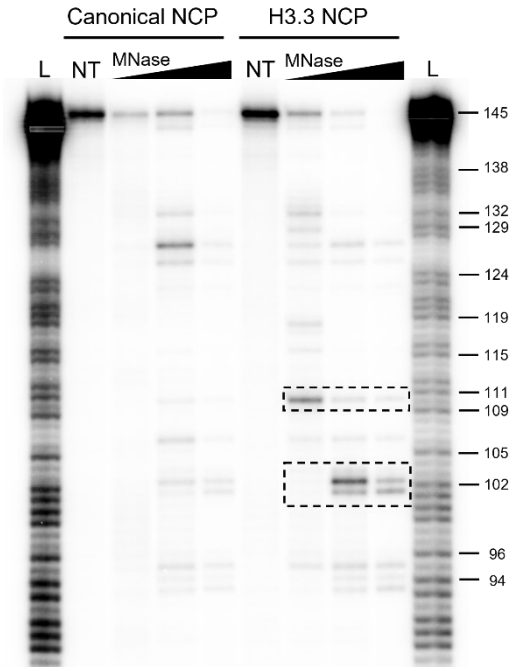

Figure 7. Micrococcal nuclease (Mnase) digestion of canonical and H3.3 variant NCPs. Canonical and H3.3 NCPs were treated with increasing amounts of Mnase. The non-treated (NT) samples serve as a negative control where no Mnase was added. The digestion results were resolved by denaturing PAGE. Lane L is a size ladder created by performing the Maxam-Gilbert sequencing reaction (A+G) on the Widom 601 "I strand". Cleavage sites that are observed exclusively in H3.3 NCPs are indicated by dashed boxes.

Together, the HRF and MNase digestion data for the slower-migrating species are consistent with previous studies of a hexasome, which lacks one copy of the H2A/H2B dimer and wraps only 112 bp of DNA [33,34]. Notably, the 102-mer and 103-mer fragments observed by MNase digestion likely result from transient unwrapping of the DNA near the entry/exit region in hexasomes. The faster-migrating species, which co-migrates with canonical NCPs via native PAGE, is consistent with an octasome, which contains the full complement of histone proteins.

3.6 Repair fingerprint of UDG and SMUG1 on H3.3 octasome and hexasome species

The activities of UDG and SMUG1 on the purified H3.3 octasome and hexasome species were next examined (Figure 8, Figure S6). U excision by UDG in H3.3 octasome NCPs (Figure

8A, pink bars) has enhanced activity compared to canonical NCPs (Figure 8, black bars) at sites 63, 94, 95, 106, 109, and 115. In other locations, enhancement of UDG activity is also observed although the absolute values are small, such as sites 110 and 122.

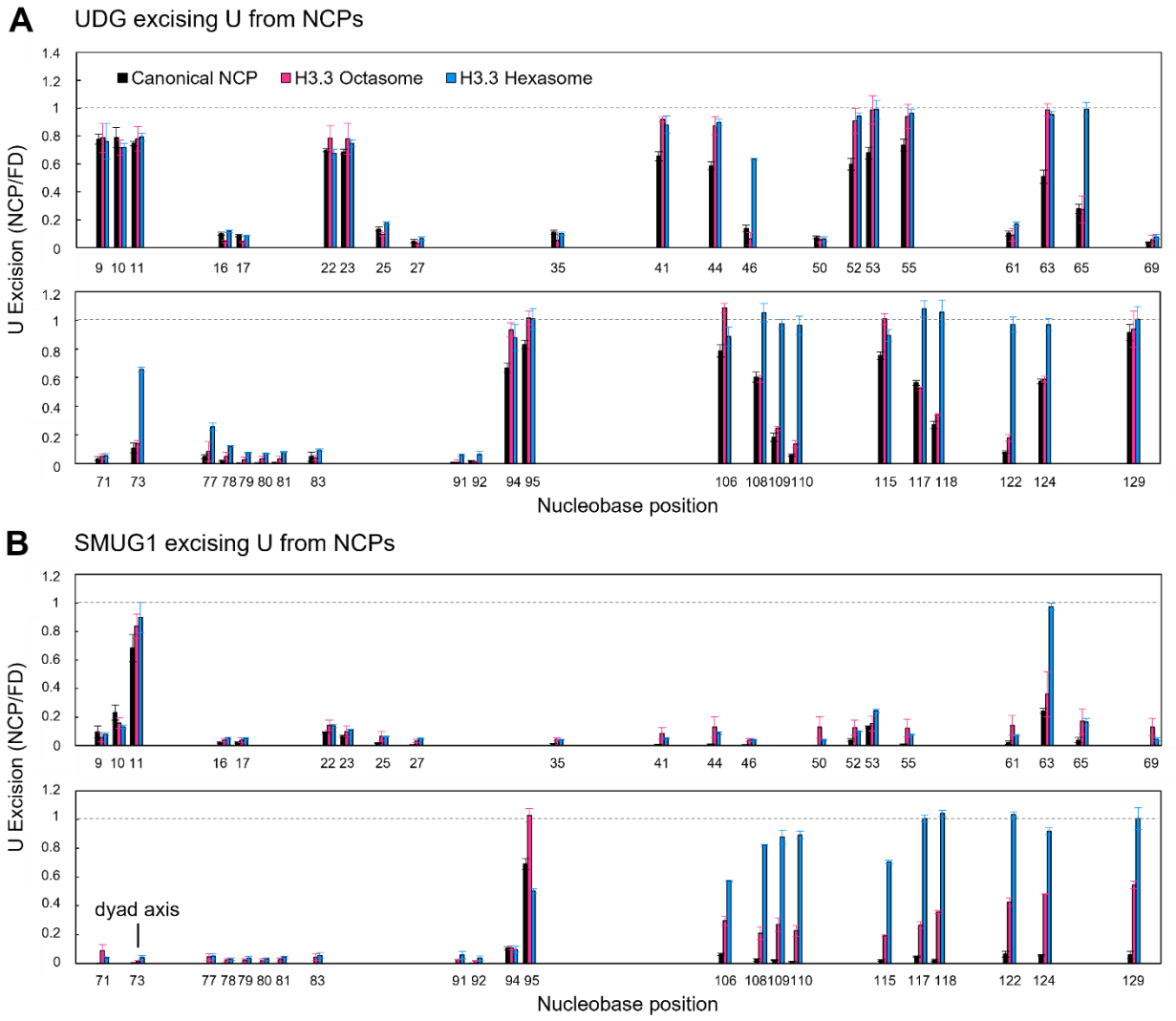

Figure 8. Excision of U from NCPs containing global C to U substitution after incubation with UDG (A) or SMUG1 (B). At each U site, the ratio of product yield in NCPs to that in duplex DNA is plotted versus nucleobase position (canonical NCPs, black; H3.3 octasome NCPs, pink; H3.3 hexasome NCPs, blue). A ratio of 1, indicated by a dotted line, represents a case in which excision of U from NCPs is as efficient as in duplex DNA. The dyad axis is indicated at position 73. Error bars represent standard error (n=3).

In H3.3 hexasome NCPs (Figure 8A, blue bars), sites that have enhanced UDG activity are 44, 46, 63, 65, 73, 77, 78-81, and the 108-124 region. H3.3 hexasome species leads to enhanced

UDG activity compared to canonical NCPs, at more sites than H3.3 octasome. H3.3 hexasome NCPs also alleviate the inhibition of UDG at site 73.

U excision by SMUG1 in H3.3 octasome NCPs (Figure 8B, pink bars) has notably enhanced activity levels compared to canonical NCPs at sites 95, 106 and the 109-129 region. SMUG1 excision of U in H3.3 hexasome NCPs (Figure 8B, blue bars) also shows enhanced activity in the 106-129 region as well as site 63. The 106-129 region has a 9.5 to 89-fold increase in activity levels, the most drastic effect of the variant NCPs examined here (Table S3). Contrasting to H3.3 octasome, in the H3.3 hexasome site 95 displays a decrease in SMUG1 activity. In contrast to excision by UDG, suppression of SMUG1 activity at the dyad axis is not affected by H3.3 octasome or hexasome NCPs.

Figure S7 compares directly UDG and SMUG1 excision activity on the purified octasome species of H3.3 and the dual variant H3.3/H2A.Z NCPs. This data compares glycosylase activity when the full complement of eight core histone proteins is present. For UDG, there are several lesion sites that are more readily excised in the dual-variant NCPs: 16, 17, 25, 27, 35, 46, 65, 117, 118, and 124. For SMUG1, the overall pattern is similar to that seen in Figure 5A but the levels of U excision in the region from site 106 to 129 in H3.3 NCPs is diminished. Therefore, while SMUG1 has enhanced excision activity in this region even in octasomes species, the loss of an H2A/H2B dimer further enhances glycosylase activity.

3.7 Mapping of U excision from NCPs by UDG and SMUG1

To visualize differences in excision activity by UDG (Figure 9A) or SMUG1 (Figure 9B) on variant NCPs, U sites were categorized and mapped on the canonical NCP structure. U sites were categorized into three groups based on the difference in excision ratios between the respective

variant and canonical NCPs: differences less than 0.1 (Figure 9, blue), between 0.1 and 0.3 (Figure 9, orange), and greater than 0.3 (Figure 9, pink).

UDG exhibits a range of significant activities in the H2A.Z/H3.3 NCP while SMUG1 has limited differences in activity compared to canonical NCPs. The NCP maps for both UDG and SMUG1 also show a variety of levels of activity enhancement in the H3.3 octasome NCP. In the H3.3 hexasome, lesions with the greatest enhancement in excision (pink), are clustered in the region where H2A/H2B dimer is absent in the hexasome NCP.

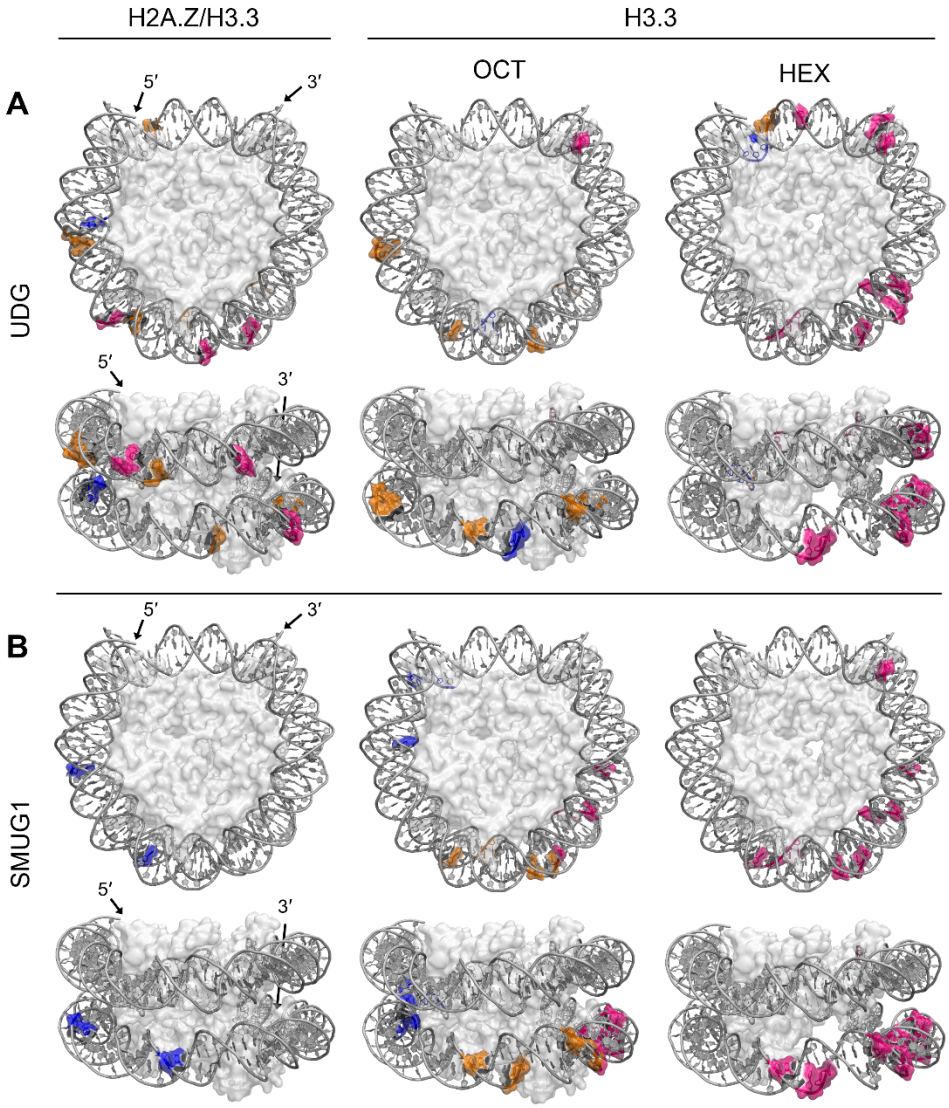

Figure 9. Structure of 601 NCP (3lz0) with U sites highlighted to represent differences in excision levels by UDG (A) or SMUG1 (B) in variant NCPs relative to canonical. Differences in U excision

values (NCP/FD; from Figures 4A, 5A, and 8) between H2A.Z/H3.3 NCPs, H3.3 octamer NCPs (OCT), or H3.3 hexamer NCPs (HEX) and canonical NCPs are highlighted. Differences less than 0.1, between 0.1 and 0.3, and greater than 0.3 are shown in blue, orange, and pink respectively. The 5′- and 3′-ends of the U-containing strand are labeled accordingly. One copy of H2A/H2B dimer near which UDG and SMUG1 activity is restored, is omitted from the hexasome NCP maps. Only sites with significant differences ($p<0.05$) were highlighted. Each NCP map has a front view and a side view where the NCP has been rotated 90° into the page.

4. Discussion

In this work, we constructed a global repair profile of UDG and SMUG1 in the context of canonical, H3.3, and H2A.Z/H3.3 NCPs. In canonical NCPs, U excision by UDG generally correlates with solution accessibility and translational positioning. This result is consistent with previous observations in NCPs [35,36] and *in vivo* evidence that nucleobase damage accumulates at the dyad axis region leading to high mutation frequency [37,38]. The low activity levels observed for SMUG1 excision of U from canonical NCPs are also consistent with previous data [16], which may be due to the invasive nature of SMUG1 binding as revealed in a co-crystal structure with duplex (*vide infra*) [39]. While canonical histones pose challenges to repair enzymes because they bind to and physically sequester DNA, histone variants, important for gene regulation and maintaining genomic stability [40], may alleviate some of the burden by altering the physical accessibility of damage sites.

Our results indicate that the presence of both H2A.Z/H3.3 facilitates UDG activity, while H3.3 facilitates both UDG and SMUG1 activity. Regarding H3.3, both the octasome and hexasome species contribute to this facilitated excision. Furthermore, the H3.3 NCPs have a 60:40 hexasome to octasome composition and the weighted average of excision ratios from purified H3.3 octasome and hexasome species is consistent with those observed for H3.3 NCPs at each position.

The H3.3 hexasome NCPs exhibit enhanced UDG and SMUG1 activity in the 3′-end region. At sites 106-129, enhancement of SMUG1 activity is much more prominent in the H3.3

hexasome NCPs than octasomes. This result is consistent with the loss of the H2A/H2B dimer in the hexasome species [33,34]. While the hexasome wraps about 112 bp of DNA, enhancement observed at sites such as 106, 108, 109, and 110 can be explained by transient asymmetric unwrapping from the hexasome core. This interpretation is supported by MNase digestion data that shows the 102- and 103-mer fragments. The loss of the H2A/H2B dimer does not appear to affect the rest of the NCP structure based on the observation that excision activity at sites other than the 3′-end region remains the same compared to canonical NCPs, with a few exceptions. Indeed, previous structural analysis of hexasome NCPs has shown that the remaining structure is similar to that of the canonical NCP [33].

One position of particular interest that displays differing SMUG1 excision levels in the H3.3 octasome and hexasome species is site 95. At this site, SMUG1 activity is enhanced and suppressed in the H3.3 octasome and hexasomes, respectively. Site 95 is one of the few sites that is well excised by SMUG1 in canonical NCPs, potentially because it is highly solution accessible. But knowing that the overall structure of the hexasome NCP is retained, this loss of activity may be due to concomitant changes in histone tails with the loss of the H2A/H2B dimer. When the H2A/H2B dimer is lost, the H3 tails experience increased conformational dynamics [41]. H3 tails in a hexasome NCP were shown to adopt asymmetric conformations where the tail closest to the missing H2A/H2B dimer resembles the conformation of a tetrasome, while the other resembles the conformation of a canonical NCP.

Histone tails may also make other contributions to repair. Deletion of the N-terminal tails of H2A and H3 in *S. cerevisiae* sensitizes the cells to alkylating agents and leads to decreased expression of the Mag1 glycosylase mRNA [42]. Acetylation of lysines in histone tails is known to affect chromatin compaction. However, while in the presence of a bulky DNA lesion H2B

becomes entrapped and cannot carry out its regulatory roles when acetylated or deacetylated [43,44]. Lysine rich histone tails have been shown to react with and form DNA-protein crosslinks with abasic sites [45-47] and some damaged nucleobases [48-53]. Post-translational modification of histone tails has also been shown to facilitate BER by preventing crosslinking [54]. Based on phenol-chloroform extractions there is no evidence for stable protein crosslink formation under the experimental conditions used in this work. Nevertheless, histone tail interactions may still play a role in the observed glycosylase activity.

While at some positions the H2A.Z/H3.3 and/or H3.3 variants have a sizable impact on the excision activity of glycosylases, some changes are small but still statistically significant. For instance, at site 78, UDG exhibits a 6-fold increase in excision of U from H3.3 hexasome NCPs compared to canonical NCPs. Excision of U from H3.3 hexasomes is still low at position 78 compared to other nucleobase positions, but this observed enhancement of activity could potentially be significant when amplified in biological processes.

We have shown that the double-variant H2A.Z/H3.3 facilitates UDG excision activity. Nucleosome mapping in cells suggests H2A.Z increases accessibility of transcription factor binding sites and can regulate gene expression in certain promoter locations [55]. H2A.Z/H3.3 double-variant NCPs are also known to be enriched at transcription start sites and to provide access to transcription factors. In fact, H2A.Z/H3.3 NCPs and transcription factor forkhead box A1 (FOXA1) have been shown to shape the chromatin landscape in the context of DNA demethylation in nucleosome arrays [56]. Enhanced glycosylase activity in NCPs containing these variants may be beneficial to regulate and facilitate repair as they are enriched in actively transcribed genes.

We speculate that the increase in stability of NCPs (i.e., lack of hexasomes) that contain both H2A.Z and H3.3 derives from structural alterations that occur relative to NCPs containing

only H3.3. ~~While direct structural information is not available for the dual-variant NCP, the~~The H2A family of variants, including H2A.Z, exhibit sequence divergence from H2A in the docking domain, L1 loop, and acidic patch [57]. It has been shown that these sequence changes in H2A.Z stabilize nucleosomes [58]. The crystal structure of H2A.Z/H3.3 nucleosomes and thermal stability assays show~~s~~ that the incorporation of H3.3 does not affect NCP stability compared to H2A.Z nucleosomes [59]. Furthermore, native PAGE analysis of H2A.Z/H3.3 NCPs reconstituted *in vitro* shows that H2A.Z dominates the translational positioning of DNA, relative to H3.3 ~~and H2A.Z dual variant~~ nucleosomes and H2A.Z NCPs [32]. We speculate that in a similar manner the H2A.Z variant stabilizes interactions within the octamer core of the dual-variant NCPs which prevents hexasome formation.

It is interesting to note that while both glycosylases excise U and are members of the UDG superfamily of glycosylases, UDG and SMUG1 display different activities on NCPs. This difference in activity may be due to differences in their size, shape, binding, and/or catalytic mechanism. The intercalating region of SMUG1 contains an α helix unique to SMUG1 known as the "helical wedge" [39]. This component is thought to be responsible for distortion of the DNA to access the target lesion. The more invasive nature of the binding of SMUG1 may render this glycosylase more susceptible to the physical challenges posed by an NCP than UDG.

SMUG1 is not cell cycle regulated but rather is expressed at constant, low levels [6059~~59~~]. It has also been shown to localize predominantly in nucleoli, where there are regions of both condensed and decondensed chromatin [6059~~59~~]. SMUG1 also has a broader substrate specificity than UDG [6059~~59~~,610~~10~~]. UDG, on the other hand, is upregulated during S-phase. It is worth noting that the *E.coli* UDG used in the present work lacks the N-terminal domain found in the human homolog UNG2, which has been shown to be responsible for interacting with proliferating cell

nuclear antigen (PCNA) and replication protein A2 (RPA2) at replication foci [621]. Therefore, while the data reported here reflect the ability of SMUG1 and UDG to excise U from an NCP, the activity of these glycosylases may be modulated by cellular conditions or factors as part of an access-repair-restore model [15]. For instance, chromatin remodelers may alter the accessibility of the target lesions. Human cells have also been reported to contain a factor, lower in molecular weight than chromatin remodeling complexes, that facilitates excision of thymine glycol lesions from NCPs by the NTHL1 glycosylase [6332]. The UV-damaged DNA binding protein (UV-DDB), which is known to serve as a damage sensor in global genomic nucleotide excision repair (NER), has also recently been shown to stimulate 8-oxo-guanine glycosylase (OGG1) [6433] and MUTYH glycosylase [654] activity on oligonucleotides . Cellular conditions may also alter the structure and dynamics of the NCP itself [6655,6766].

5. Conclusions

The global repair profiles presented here provide a description of the inherent ability of two glycosylases to catalyze removal of U from the fundamental unit of packaging in chromatin. The results demonstrate enhanced U excision by two glycosylases in presence of histone variants: SMUG1 from H3.3 variant NCPs and UDG from H2A.Z/H3.3 and H3.3NCPs. Further studies will reveal how other cellular factors, conditions, and higher-order packaging contribute to the role of histone variants in DNA repair. Together these findings contribute to our overall understanding of BER in chromatin and the impact of DNA damage and repair on mutagenesis and genomic integrity.

CRediT authorship contribution statement

Conceptualization, C.L., S.D.; Investigation, C.L.; Formal analysis, K.L.R.; Writing – Original Draft and Review & Editing, C.L., K.L.R., S.D.; Supervision, S.D.

Acknowledgments

This research was supported by the National Science Foundation (MCB-1817417) and K.L.R. was supported by a National Institute of Environmental Health Sciences training grant (T32ES007272).

Conflict of interest statement

The authors declare that there are no conflicts of interest.

Appendix A. Supporting information

Supplementary data associated with this article can be found in the online version.

REFERENCES

[1] K. Luger, A.W. Mader, R.K. Richmond, D.F. Sargent, T.J. Richmond, Crystal structure of the nucleosome core particle at 2.8 A resolution, Nature 389 (1997) 251-260.
[2] J. Jin, Y. Cai, B. Li, R.C. Conaway, J.L. Workman, J.W. Conaway, T. Kusch, In and out: histone variant exchange in chromatin, Trends Biochem. Sci. 30 (2005) 680-687.
[3] N. Gevry, H.M. Chan, L. Laflamme, D.M. Livingston, L. Gaudreau, p21 transcription is regulated by differential localization of histone H2A.Z, Genes Dev. 21 (2007) 1869-1881.
[4] E. Szenker, D. Ray-Gallet, G. Almouzni, The double face of the histone variant H3.3, Cell Res. 21 (2011) 421-434.
[5] C.M. Weber, S. Henikoff, Histone variants: dynamic punctuation in transcription, Genes Dev. 28 (2014) 672-682.
[6] J.Y. Fan, F. Gordon, K. Luger, J.C. Hansen, D.J. Tremethick, The essential histone variant H2A.Z regulates the equilibrium between different chromatin conformational states, Nat. Struct. Biol. 9 (2002) 172-176.
[7] R.K. Suto, M.J. Clarkson, D.J. Tremethick, K. Luger, Crystal structure of a nucleosome core particle containing the variant histone H2A.Z, Nat. Struct. Biol. 7 (2000) 1121-1124.
[8] C. Jin, G. Felsenfeld, Nucleosome stability mediated by histone variants H3.3 and H2A.Z, Genes & Development 21 (2007) 1519-1529.
[9] A. Li, Y. Yu, S.C. Lee, T. Ishibashi, S.P. Lees-Miller, J. Ausió, Phosphorylation of histone H2A.X by DNA-dependent protein kinase is not affected by core histone acetylation, but it alters nucleosome stability and histone H1 binding, J. Biol. Chem. 285 (2010) 17778-17788.

[10] I. Maze, K.M. Noh, A.A. Soshnev, C.D. Allis, Every amino acid matters: essential contributions of histone variants to mammalian development and disease, Nat. Rev. Genet. 15 (2014) 259-271.
[11] D. Bano, A. Piazzesi, P. Salomoni, P. Nicotera, The histone variant H3.3 claims its place in the crowded scene of epigenetics, Aging 9 (2017) 602-614.
[12] S. Juhász, A. Elbakry, A. Mathes, M. Löbrich, ATRX Promotes DNA Repair Synthesis and Sister Chromatid Exchange during Homologous Recombination, Mol. Cell 71 (2018) 11-24.e7.
[13] S. Adam, S.E. Polo, G. Almouzni, Transcription Recovery after DNA Damage Requires Chromatin Priming by the H3.3 Histone Chaperone HIRA, Cell 155 (2013) 94-106.
[14] C. Jin, C. Zang, G. Wei, K. Cui, W. Peng, K. Zhao, G. Felsenfeld, H3.3/H2A.Z double variant-containing nucleosomes mark 'nucleosome-free regions' of active promoters and other regulatory regions, Nat. Genet. 41 (2009) 941-945.
[15] S.E. Polo, G. Almouzni, Chromatin dynamics after DNA damage: The legacy of the access-repair-restore model, DNA Repair 36 (2015) 114-121.
[16] C. Li, S. Delaney, Histone H2A Variants Enhance the Initiation of Base Excision Repair in Nucleosomes, ACS Chem. Biol. 14 (2019) 1041-1050.
[17] L. Alsøe, A. Sarno, S. Carracedo, D. Domanska, F. Dingler, L. Lirussi, T. SenGupta, N.B. Tekin, L. Jobert, L.B. Alexandrov, A. Galashevskaya, C. Rada, G.K. Sandve, T. Rognes, H.E. Krokan, H. Nilsen, Uracil Accumulation and Mutagenesis Dominated by Cytosine Deamination in CpG Dinucleotides in Mice Lacking UNG and SMUG1, Sci. Rep. 7 (2017) 7199.
[18] D. Vasudevan, E.Y.D. Chua, C.A. Davey, Crystal Structures of Nucleosome Core Particles Containing the '601' Strong Positioning Sequence, J. Mol. Biol. 403 (2010) 1-10.
[19] K. Bilotti, M.E. Tarantino, S. Delaney, Human Oxoguanine Glycosylase 1 Removes Solution Accessible 8-Oxo-7,8-dihydroguanine Lesions from Globally Substituted Nucleosomes Except in the Dyad Region, Biochemistry 57 (2018) 1436-1439.
[20] K. Luger, T.J. Rechsteiner, T.J. Richmond, Expression and purification of recombinant histones and nucleosome reconstitution, Methods Mol. Biol. 119 (1999) 1-16.
[21] K. Luger, T.J. Rechsteiner, T.J. Richmond, Preparation of nucleosome core particle from recombinant histones, Meth. Enzymol. 304 (1999) 3-19.
[22] J.M. Hinz, Y. Rodriguez, M.J. Smerdon, Rotational dynamics of DNA on the nucleosome surface markedly impact accessibility to a DNA repair enzyme, Proc. Natl. Acad. Sci. 107 (2010) 4646.
[23] H.A. Cole, J.M. Tabor-Godwin, J.J. Hayes, Uracil DNA Glycosylase Activity on Nucleosomal DNA Depends on Rotational Orientation of Targets, J. Biol. Chem. 285 (2010) 2876-2885.
[24] L.C. Olsen, R. Aasland, C.U. Wittwer, H.E. Krokan, D.E. Helland, Molecular cloning of human uracil-DNA glycosylase, a highly conserved DNA repair enzyme, EMBO J. 8 (1989) 3121-3125.
[25] G. Xiao, M. Tordova, J. Jagadeesh, A.C. Drohat, J.T. Stivers, G.L. Gilliland, Crystal structure of Escherichia coli uracil DNA glycosylase and its complexes with uracil and glycerol: structure and glycosylase mechanism revisited, Proteins 35 (1999) 13-24.
[26] R. Das, A. Laederach, S.M. Pearlman, D. Herschlag, R.B. Altman, SAFA: semi-automated footprinting analysis software for high-throughput quantification of nucleic acid footprinting experiments, RNA 11 (2005) 344-354.
[27] S.S. Jain, T.D. Tullius, Footprinting protein–DNA complexes using the hydroxyl radical, Nat. Protoc. 3 (2008) 1092.

[28] J.J. Hayes, T.D. Tullius, A.P. Wolffe, The structure of DNA in a nucleosome, Proc. Natl. Acad. Sci. 87 (1990) 7405-7409.
[29] P.T. Lowary, J. Widom, New DNA sequence rules for high affinity binding to histone octamer and sequence-directed nucleosome positioning, J. Mol. Biol. 276 (1998) 19-42.
[30] E.Y.D. Chua, D. Vasudevan, G.E. Davey, B. Wu, C.A. Davey, The mechanics behind DNA sequence-dependent properties of the nucleosome, Nucleic Acids Res. 40 (2012) 6338-6352.
[31] T.T. Ngo, Q. Zhang, R. Zhou, J.G. Yodh, T. Ha, Asymmetric unwrapping of nucleosomes under tension directed by DNA local flexibility, Cell 160 (2015) 1135-1144.
[32] A. Thakar, P. Gupta, T. Ishibashi, R. Finn, B. Silva-Moreno, S. Uchiyama, K. Fukui, M. Tomschik, J. Ausio, J. Zlatanova, H2A.Z and H3.3 Histone Variants Affect Nucleosome Structure: Biochemical and Biophysical Studies, Biochemistry 48 (2009) 10852-10857.
[33] Y. Arimura, H. Tachiwana, T. Oda, M. Sato, H. Kurumizaka, Structural Analysis of the Hexasome, Lacking One Histone H2A/H2B Dimer from the Conventional Nucleosome, Biochemistry 51 (2012) 3302-3309.
[34] D. Kato, A. Osakabe, Y. Arimura, Y. Mizukami, N. Horikoshi, K. Saikusa, S. Akashi, Y. Nishimura, S.-Y. Park, J. Nogami, K. Maehara, Y. Ohkawa, A. Matsumoto, H. Kono, R. Inoue, M. Sugiyama, H. Kurumizaka, Crystal structure of the overlapping dinucleosome composed of hexasome and octasome, Science 356 (2017) 205-208.
[35] B.C. Beard, S.H. Wilson, M.J. Smerdon, Suppressed catalytic activity of base excision repair enzymes on rotationally positioned uracil in nucleosomes, Proc. Natl. Acad. Sci. 100 (2003) 7465-7470.
[36] Y. Rodriguez, M.J. Smerdon, The structural location of DNA lesions in nucleosome core particles determines accessibility by base excision repair enzymes, J. Biol. Chem. 288 (2013) 13863-13875.
[37] P. Mao, A.J. Brown, E.P. Malc, P.A. Mieczkowski, M.J. Smerdon, S.A. Roberts, J.J. Wyrick, Genome-wide maps of alkylation damage, repair, and mutagenesis in yeast reveal mechanisms of mutational heterogeneity, Genome Res. 27 (2017) 1674-1684.
[38] J. Wu, M. McKeague, S.J. Sturla, Nucleotide-Resolution Genome-Wide Mapping of Oxidative DNA Damage by Click-Code-Seq, J. Am. Chem. Soc. 140 (2018) 9783-9787.
[39] J.E.A. Wibley, T.R. Waters, K. Haushalter, G.L. Verdine, L.H. Pearl, Structure and Specificity of the Vertebrate Anti-Mutator Uracil-DNA Glycosylase SMUG1, Mol. Cell 11 (2003) 1647-1659.
[40] C. Volle, Y. Dalal, Histone variants: the tricksters of the chromatin world, Curr. Opin. Genet. Dev. 25 (2014) 8-14.
[41] E.A. Morrison, L. Baweja, M.G. Poirier, J. Wereszczynski, C.A. Musselman, Nucleosome composition regulates the histone H3 tail conformational ensemble and accessibility, Nucleic Acids Res. 49 (2021) 4750-4767.
[42] R. Meas, J.J. Wyrick, M.J. Smerdon, Nucleosomes Regulate Base Excision Repair in Chromatin, Mutat. Res. Rev. Mutat. Res. 780 (2019) 29-36.
[43] I. Fu, Y. Cai, N.E. Geacintov, Y. Zhang, S. Broyde, Nucleosome Histone Tail Conformation and Dynamics: Impacts of Lysine Acetylation and a Nearby Minor Groove Benzo[a]pyrene-Derived Lesion, Biochemistry 56 (2017) 1963-1973.
[44] I. Fu, Y. Cai, Y. Zhang, N.E. Geacintov, S. Broyde, Entrapment of a Histone Tail by a DNA Lesion in a Nucleosome Suggests the Lesion Impacts Epigenetic Marking: A Molecular Dynamics Study, Biochemistry 55 (2016) 239-242.

[45] J.T. Sczepanski, R.S. Wong, J.N. McKnight, G.D. Bowman, M.M. Greenberg, Rapid DNA–protein cross-linking and strand scission by an abasic site in a nucleosome core particle. Proc. Natl. Acad. Sci. 107 (2010) 22475.
[46] R. Wang, K. Yang, S. Banerjee, M.M. Greenberg. Rotational effects within nucleosome core particles on abasic site reactivity. Biochemistry 57 (2018) 3945-3952.
[47] C.Z. Zhou, J.T. Sczepanski, M.M. Greenberg. Mechanistic studies on histone catalyzed cleavage of apyrimidinic/apurinic sites in nucleosome core particles. J. Am. Chem. Soc. 134, (2012) 16734-16741.
[48] Ren, M.; Shang, M.; Wang, H.; Xi, Z.; Zhou, C., Histones participate in base excision repair of 8-oxodGuo by transiently cross-linking with active repair intermediates in nucleosome core particles. Nucleic Acids Res. 2021, 49, 257-268.
[49] K. Yang, D. Park, N.Y. Tretyakova, M.M. Greenberg, Histone tails decrease N7-methyl-2′-deoxyguanosine depurination and yield DNA–protein cross-links in nucleosome core particles and cells. Proc. Natl. Acad. Sci. 115 (2018) 11212-11220.
[50] M. Shang, M. Ren, C. Zhou. Nitrogen mustard induces formation of DNA–histone crosslinks in nucleosome core particles. Chem. Res. Toxicol. 32 (2019) 2517-2525.
[51] K. Yang, H. Sun, L. Lowder, S. Varadarajan, M.M. Greenberg. Reactivity of N3-methyl-2 '-deoxyadenosine in nucleosome core particles. Chem. Res. Toxicol. 32 (2019) 2118-2124.
[52] K. Yang, M.M. Greenberg. DNA-protein cross-link formation in nucleosome core particles treated with methyl methanesulfonate. Chem. Res. Toxicol. 32 (2019) 2144-2151.
[53] J. Bai, Y. Zhang, Z. Xi, M.M. Greenberg, C. Zhou. Oxidation of 8-oxo-7,8-dihydro-2′-deoxyguanosine leads to substantial DNA-histone cross-links within nucleosome core particles. Chem. Res. Toxicol. 31 (2018) 1364-1372.
[54] K. Yang, C. Prasse, M.M. Greenberg. Effect of histone lysine methylation on DNA lesion reactivity in nucleosome core particles. Chem. Res. Toxicol. 32 (2019) 910-916.
[55] L. Cole, S. Kurscheid, M. Nekrasov, R. Domaschenz, D.L. Vera, J.H. Dennis, D.J. Tremethick, Multiple roles of H2A.Z in regulating promoter chromatin architecture in human cells, Nat. Commun. 12 (2021) 2524.
[56] C.E. Deckard, D.R. Banerjee, J.T. Sczepanski, Chromatin Structure and the Pioneering Transcription Factor FOXA1 Regulate TDG-Mediated Removal of 5-Formylcytosine from DNA. J. Am. Chem. Soc. 141 (2019) 14110-14114.
[57] C. Bönish, S.B. Hake. Histone H2A Variants in Nucleosomes and Chromatin: More or Less Stable? Nucleic Acids Res. 40 (2012) 10719-10741.
[58] Y.-J. Park, P.N. Dyer, D.J. Tremethick, K. Luger. A New Fluorescence Resonance Energy Transfer Approach Demonstrates that the Histone Variant H2AZ Stabilizes the Histone Octamer Within the Nucleosome. J. Biol. Chem. 279 (2004) 24274-24282.
[59] N. Horikoshi, Y. Arimura, H. Taguchi, H. Kurumizaka. Crystal structures of heterotypic nucleosomes containing histones H2A.Z and H2A. Open Biology. 6 (2016) 160127
[60] B. Kavli, O. Sundheim, M. Akbari, M. Otterlei, H. Nilsen, F. Skorpen, P.A. Aas, L. Hagen, H.E. Krokan, G. Slupphaug, hUNG2 Is the Major Repair Enzyme for Removal of Uracil from U:A Matches, U:G Mismatches, and U in Single-stranded DNA, with hSMUG1 as a Broad Specificity Backup, J. Biol. Chem. 277 (2002) 39926-39936.
[610] H.S. Pettersen, O. Sundheim, K.M. Gilljam, G. Slupphaug, H.E. Krokan, B. Kavli, Uracil-DNA glycosylases SMUG1 and UNG2 coordinate the initial steps of base excision repair by distinct mechanisms, Nucleic Acids Res. 35 (2007) 3879-3892.

[621] M. Otterlei, E. Warbrick, T.A. Nagelhus, T. Haug, G. Slupphaug, M. Akbari, P.A. Aas, K. Steinsbekk, O. Bakke, H.E. Krokan, Post-Replicative Base Excision Repair in Replication Foci, EMBO J. 18 (1999) 3834-3844.
[632] R.L. Maher, C.G. Marsden, A.M. Averill, S.S. Wallace, J.B. Sweasy, D.S. Pederson, Human cells contain a factor that facilitates the DNA glycosylase-mediated excision of oxidized bases from occluded sites in nucleosomes, DNA Repair 57 (2017) 91-97.
[643] S. Jang, N. Kumar, E.C. Beckwitt, M. Kong, E. Fouquerel, V. Rapić-Otrin, R. Prasad, S.C. Watkins, C. Khuu, C. Majumdar, S.S. David, S.H. Wilson, M.P. Bruchez, P.L. Opresko, B. Van Houten, Damage sensor role of UV-DDB during base excision repair, Nat. Struct. Mol. Biol. 26 (2019) 695-703.
[654] S. Jang, M.A. Schaich, C. Khuu, B.L. Schnable, C. Majumdar, S.C. Watkins, S.S. David, B. Van Houten, Single Molecule Analysis Indicates Stimulation of MUTYH by UV-DDB Through Enzyme Turnover, Nucleic Acids Res. 49 (2021) 8177-8188.
[665] T.-H. Lee, Physical Chemistry of Epigenetics: Single-Molecule Investigations, J. Phys. Chem. B 123 (2019) 8351-8362.
[676] B. Fierz, M.G. Poirier, Biophysics of chromatin dynamics, Annu Rev Biophys. 48 (2019) 321-345.